ASSOCIATED CONTENT

Supporting Information.

Experimental Methods

Preparation of FA-based bromide perovskite precursor solutions. For R = 1, 1 mmol (0.367g) of $PbBr_2$ (99.999%, Alfa aesar) and 1 mmol (0.125g) of FABr (Dyesol) were dissolved in 1ml of dimethyl sulfoxide (DMSO, anhydrous, 99.9%, Sigma Aldrich) at room temperature. For off-stoichiometric precursor solutions, we fixed the amount of $PbBr_2$ to 1 mmol (0.367g), and adjusted the amount of FABr. (1.2 mmol for R = 1.2, 1.5 mmol for R = 1.5, 2 mmol for R = 2, and 3 mmol for R = 3)

Thin film fabrication. The precursor solutions were spin-coated on the glass substrates with 1000 rpm for 5 s (acceleration = 500 rpm/s) and 3000 rpm for 40 s (acceleration = 1000 rpm/s). Some amounts of chlorobenzene were dropped on to the substrate after 20 s in the second step, and the as-spun films were annealed at desired temperatures for 10 min.

Characterization. The light absorbance was measured by UV/VIS/NIR spectrophotometer (SolidSpec-3700) and the steady-state photoluminescence was measured by F-7000 FL Spectrophotometer. Photoluminescence quantum yield (PLQY) was measured by Quantaurus-QY Absolute PL quantum yield spectrometer (Hamamatsu, C11347), using integral sphere. Samples were excited by Xenon lamp with monochromator (selected wavelength at 420 nm with 10nm bandwidth), and the scattered excitation and emission lights in the integral sphere were collected together into the fiber optic coupled spectrometer. The excitation and emission spectrum were collected sequentially for a reference (soda-lime glass) and for the sample. By the definition,

PLQY is determined by the ratio of the number of emission photons over the number of absorbed photons, which can be expressed by the following equation,

$$\mathrm{PLQY} = \frac{R_{em} - S_{em}}{R_{exc} - S_{exc}}$$

S_{em} and S_{exc} are the integrated intensity of the emission and excitation region, respectively, for the sample, and likewise, R_{em} and R_{exc} for the reference.

Time-resolved photoluminescence lifetime (TRPL) was measured with different monitoring wavelengths to obtain decay associated spectra (DAS) and time-resolved emission spectra (TRES). Decay associated spectra (DAS) was plotted by the amplitudes of each decay components with different monitoring wavelengths. X-ray diffractometry (XRD, Ultima IV, RIGAKU) was conducted using CuKα radiation (λ = 0.154 nm). FT-IR spectrum was measured by FT-IR spectrometer (Nicolet iS50, Thermo Fisher Scientific Instrument) to measure perovskite thin films on glass substrates.

First principles calculations. Using Kohn-Sham density functional theory (DFT)[1] within periodic boundary conditions, structure optimizations and electronic structure calculations were performed. The Vienna Ab initio Simulation Package (VASP)[2,3] code with projector augmented wave (PAW)[4,5] pseudopotentials were used for all the calculations where the plane-wave kinetic cutoff energy and energy convergence criteria are set to 700 eV and 10^{-5} eV. For the structure optimizations, the Perdew−Burke−Ernzerhof exchange-correlation functional revised for solids (PBEsol)[6] was employed and internal coordinates of atoms were fully relaxed until total forces on each atoms become smaller than 10^{-3} eV/Å. In order to model FA_2PbBr_4 and FA_2PbBr_4-DMSO structures, we assumed the same a_0 to that of $FAPbBr_3$ and only c_0 was optimized. The calculated lattice constants were compared to the measured values from XRD (Table S1), and both coincided

with each other. To make further agreement with experimental characterizations, we re-optimized atomic structures with fixed experimental lattice constants and adopted it for theoretical characterizations. A nonlocal hybrid functional (HSE06)[6,8], that incorporates 43% Hartree−Fock exact exchange, with spin−orbit coupling (SOC) was employed to calculate band offsets between $FAPbBr_3$ and FA_2PbBr_4-DMSO following procedure of Ref. 9. Γ-centered k-point grids of 6 point 6 was used for $FAPbBr_3$ and 6 × 6 × 2 was used for FA_2PbBr_4 and FA_2PbBr_4-DMSO.

Table S1. Theoretically calculated (DFT) and experimentally measured (XRD) lattice constants.

(Å)	$FAPbBr_3$	FA_2PbBr_4	$FAPbBr_4$-DMSO
a_0 (Theo.)	6.01	6.01 (fixed)	6.01 (fixed)
a_0 (Expt.)	6.01	unknown	unknown
c_0 (Theo.)	-	18.86	25.77
c_0 (Expt.)	-	unknown	25.48

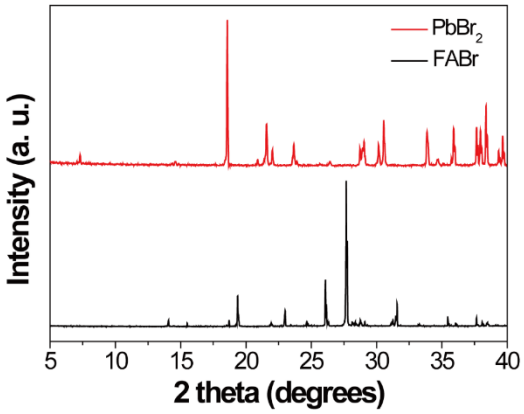

Figure S1. Powder XRD (PXRD) patterns of FABr and $PbBr_2$ powder.

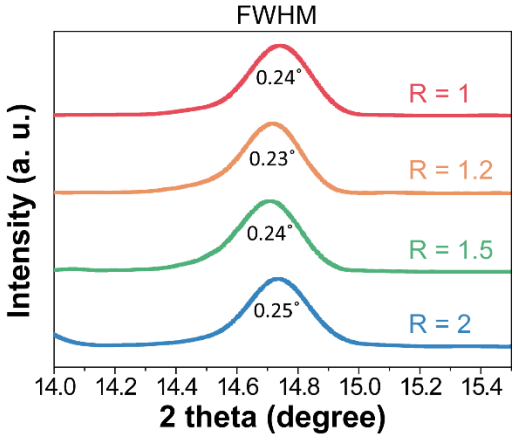

Figure S2. Zoomed-in X-ray diffraction (XRD) patterns of perovskite films with different molar ratios (R = 1, 1.2, 1.5 and 2). Those peaks indicate (100) $FAPbBr_3$. Full width at half maximum (FWHM) of peaks corresponding to each peak is shown in the graph.

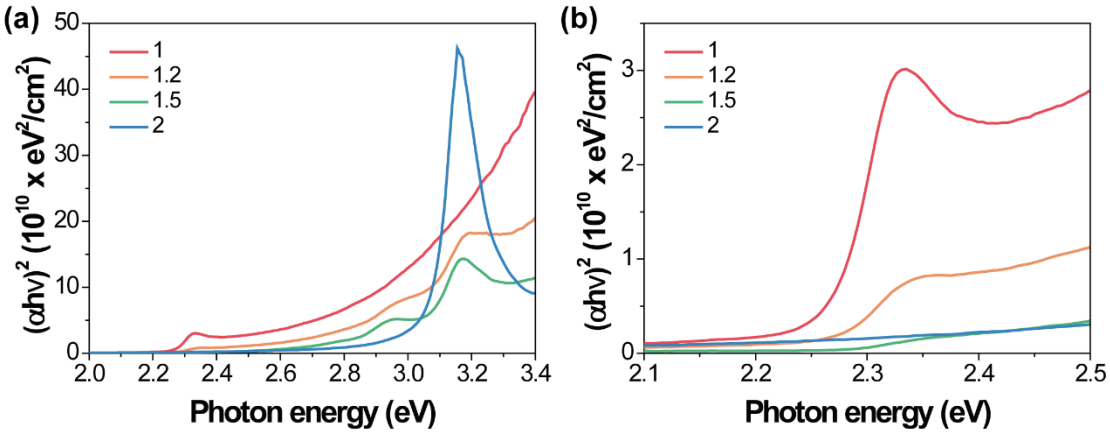

Figure S3. Tauc plot ($(\alpha hv)^2$ vs. photon energy (eV)) of 80 °C annealed perovskite films with different molar ratio (R = 1, 1.2, 1.5 and 2).

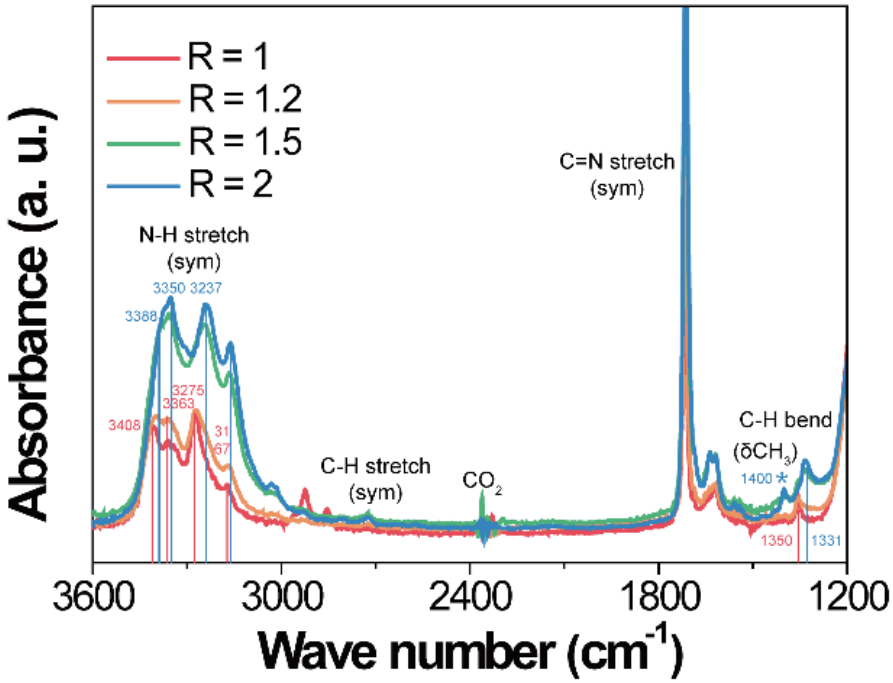

Figure S4. FT-IR spectra of 80 °C annealed perovskite films with different precursor molar ratios (R=1, 1.2, 1.5, 2). The peaks located in the range of 3400 cm^{-1} to 3100 cm^{-1} are related to N-H stretching vibrations for the FA cations. The peaks located around 2700 cm^{-1} are related to C-H stretching vibrations. The peaks located around 1700 cm^{-1} are related to C=N stretch vibrations for the FA cations. The peaks located around 1400 cm^{-1} are related to C-H bend vibrations of DMSO.

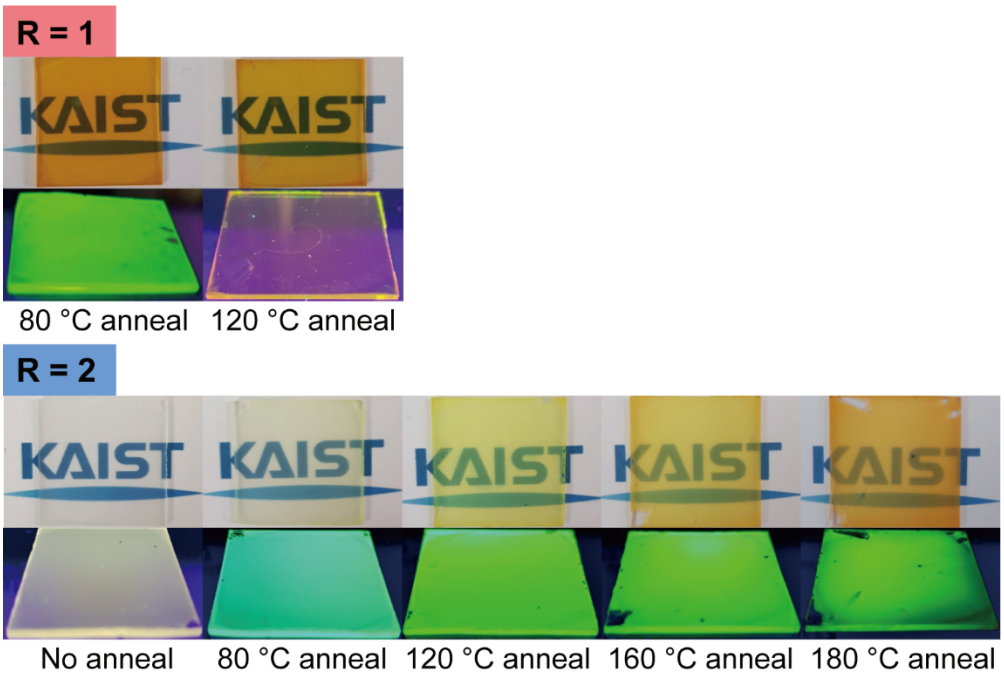

Figure S5. Digital photos of films with R = 1 and 2 subjected to different annealing temperature without and with UV light (365 nm).

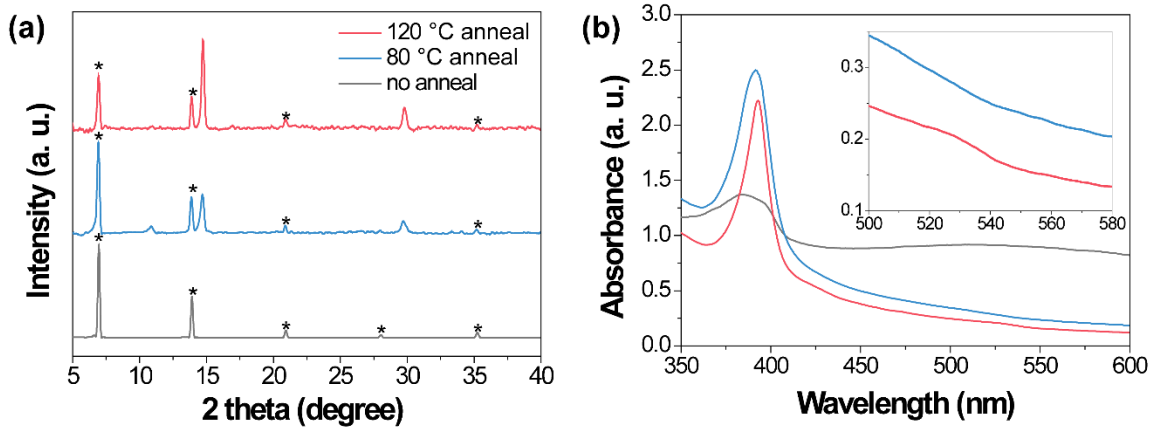

Figure S6. (a) X-ray diffraction (XRD) patterns and (b) absorption spectra of the perovskite films (R = 2) on glass substrate under different annealing conditions (no annealed, 80 °C annealed and 120 °C annealed). The marked (*) peaks represent the FA_2PbBr_4-DMSO phase.

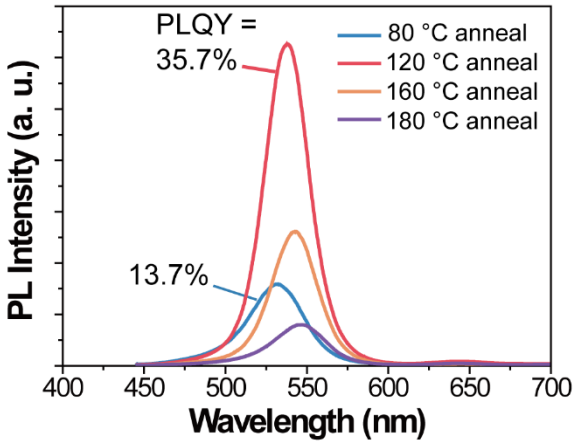

Figure S7. Steady-state PL spectra of the perovskite films (R = 2) on glass substrate with different annealing conditions (80 °C, 120 °C, 160 °C and 180 °C). Excitation wavelength is 420 nm.

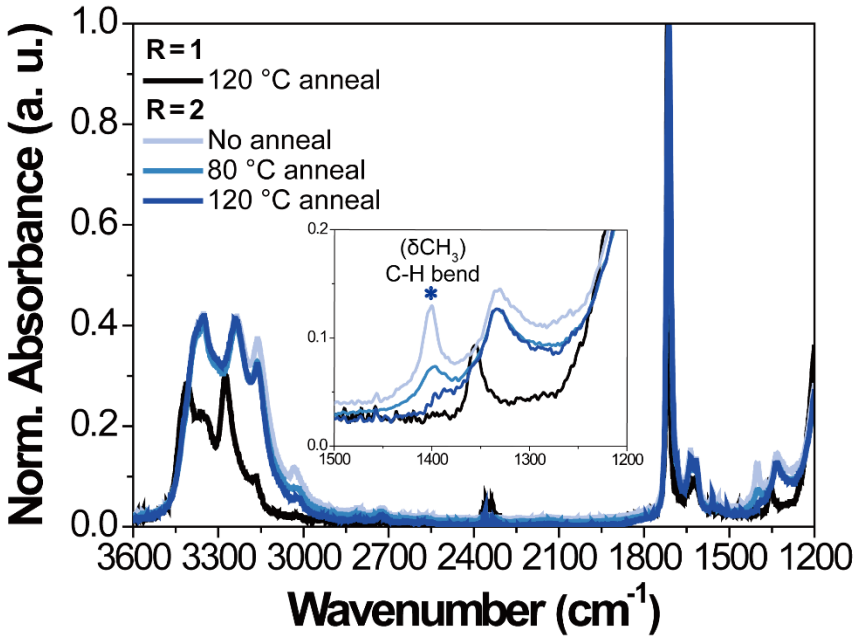

Figure S8. FT-IR spectra of films with R = 2 with various annealing temperatures (no annealing, 80 °C, 120 °C-annealed) and R = 1, 120 °C-annealed.

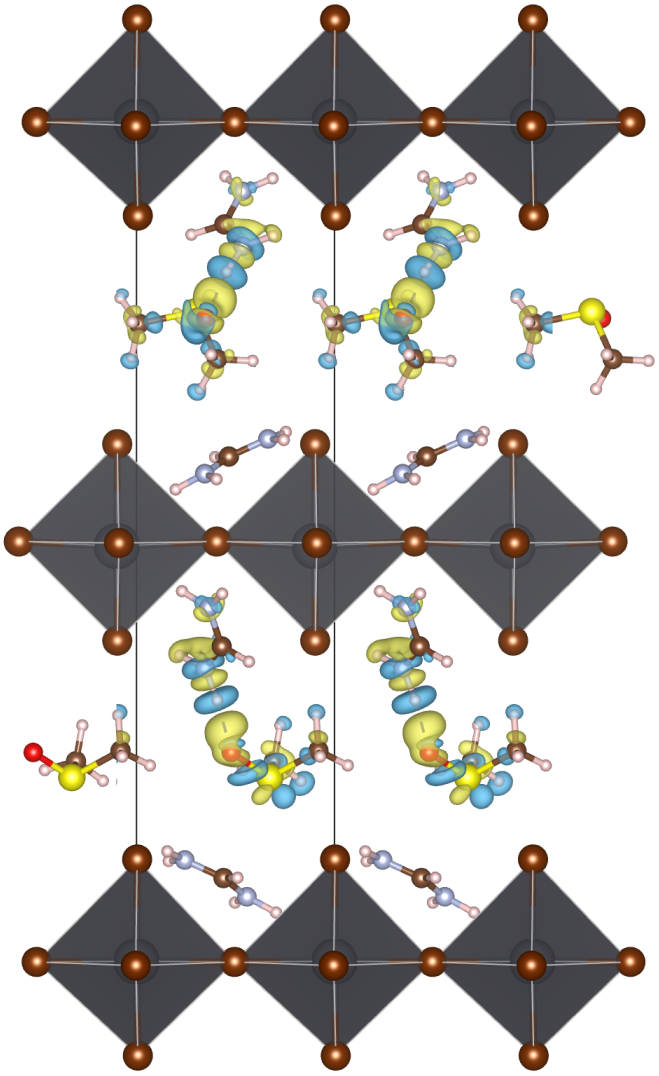

Figure S9. Isosurface plot of the charge density difference ($\Delta\rho$) which is defined as $\Delta\rho = \rho_{FA_2PbBr_4-DMSO} - \rho_{FA_2PbBr_4} - \rho_{DMSO}$). Here, $\rho_{FA_2PbBr_4-DMSO}$, $\rho_{FA_2PbBr_4}$, and ρ_{DMSO} denote charge density of $FA_2PbBr_4 - DMSO$, FA_2PbBr_4, and DMSO molecule, respectively. The electron density accumulation and depletion regions are indicated in yellow and blue.

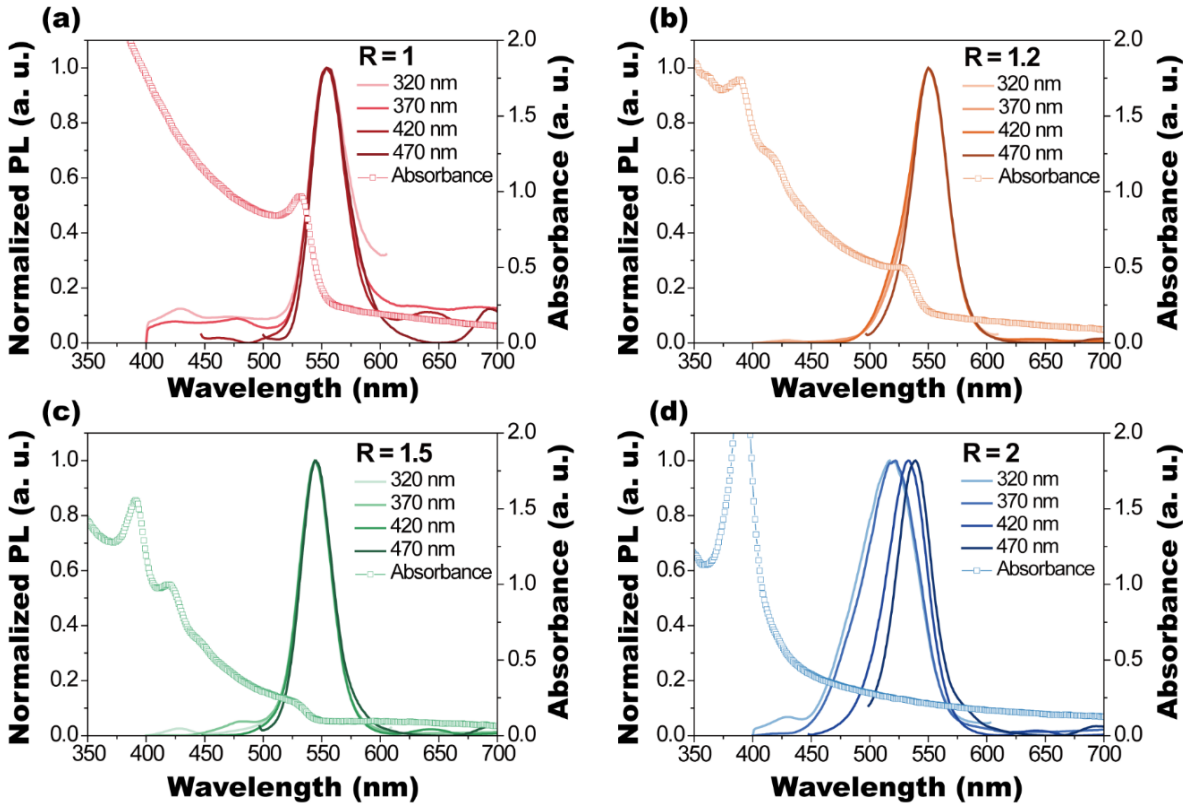

Figure S10. Normalized steady-state PL spectra with different excitation wavelengths and absorption spectra of the 80 °C-annealed perovskite films with different precursor molar ratios. (R = 1, 1.2, 1.5 and 2)

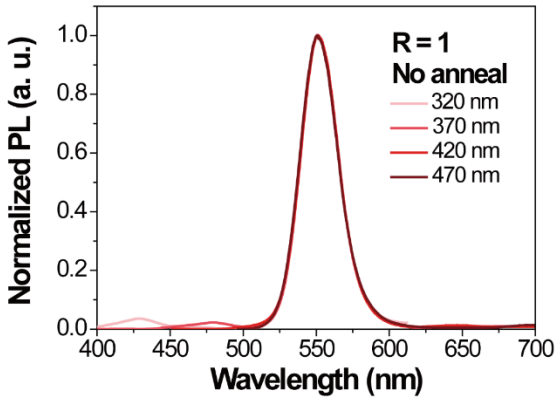

Figure S11. Normalized steady-state PL spectra with different excitation wavelengths from the non-annealed R=1 perovskite films.

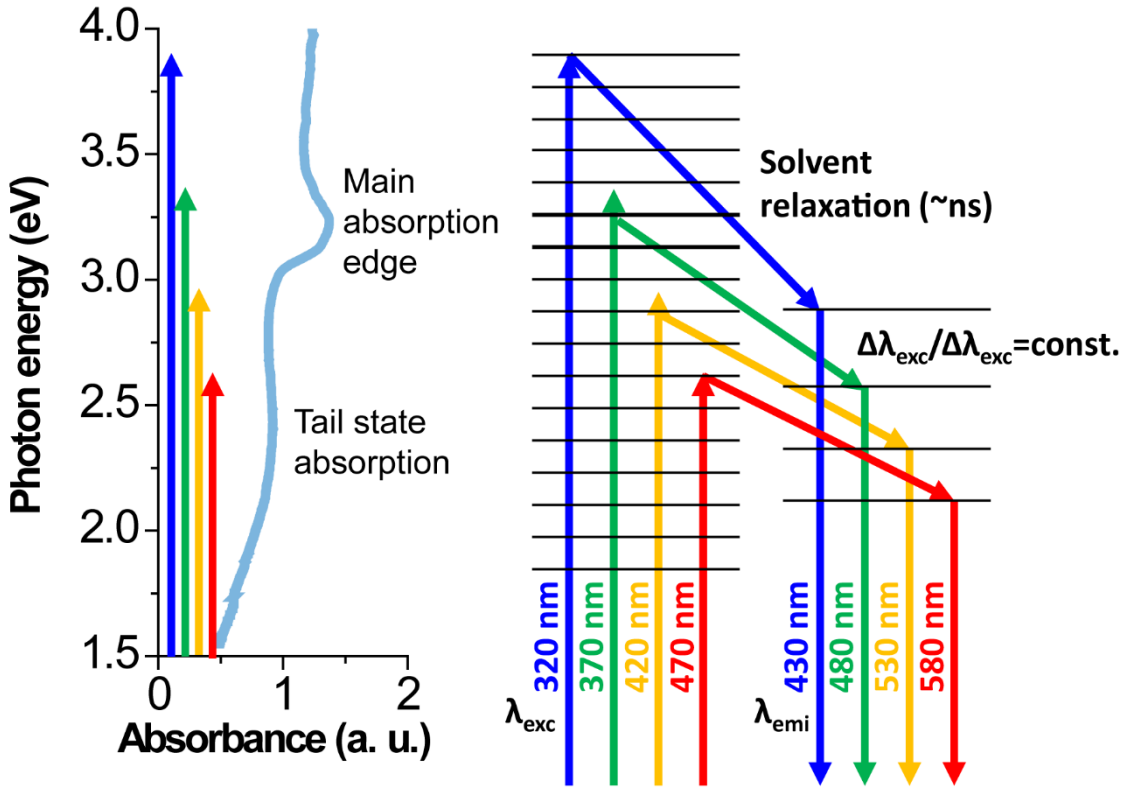

Figure S12. Schematic of the mechanism for the excitation dependent fluorescence with solvent relaxation in the non-annealed R=2 film. The schematic on the right is modified from Fig. 1 of Ref. 11.

Dipoles in polar solvent that surround fluorophores reorient or relax the dipole moment of fluorophores in excited state which is generated by light illumination. Such reorientation or relaxation process results in the stabilization of the excited state of the fluorophores (i.e., reduction of the state energy) and therefore the emission spectrum red-shifts depending on the excitation energies. This dynamic Stokes shift of emission spectrum depending on the excitation wavelength is often called as red-edge effect (REE)[10-11]. There are two prerequisites for the strong REE: (i) the solvent relaxation should occur slower than, or comparable to, the fluorescence lifetime and (ii) the fluorophore-solvent interaction energy is distributed over a large range of energy states, producing additional states of the absorbing species, which should be manifested by a long tail in the absorption spectrum. A similar mechanism may operate in our case; a polar solvent DMSO, the presence of which is necessary for the observed tunable emission characteristic, affects the energy of excited states of the 2D FA_2PbBr_4-DMSO phase. As shown in Figure S6, the R=2 film with no annealing shows a noticeable broadening in absorption spectrum, indicative of states distributed within the band gap. Additionally, solvent relaxation process in this case is expected to be slow (comparable to the fluorescence lifetime) because of the difficulty in the rotational motion of the DMSO in the 2D phase[12] compared to solvent molecules in a liquid state. Thus, strong REE was exhibited by the non-annealed R=2 film. The schematic of this mechanism is shown in Figure S11.

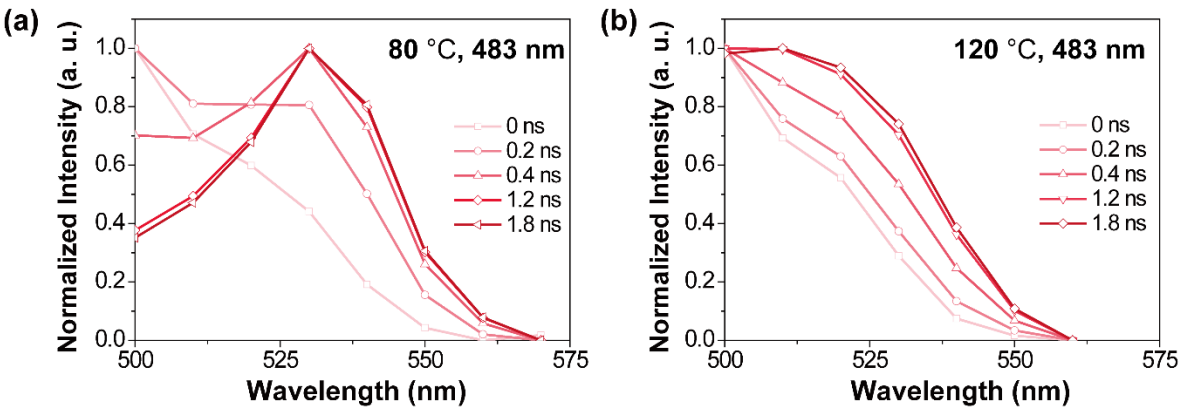

Figure S13. TRES of R = 2, 80°C and R = 2, 120°C annealed case with 483 nm excitation wavelength in the time scale between 0 ns to 1.8 ns. The 80°C-annealed film shows much faster spectral shift than the 120°C-annealed case.

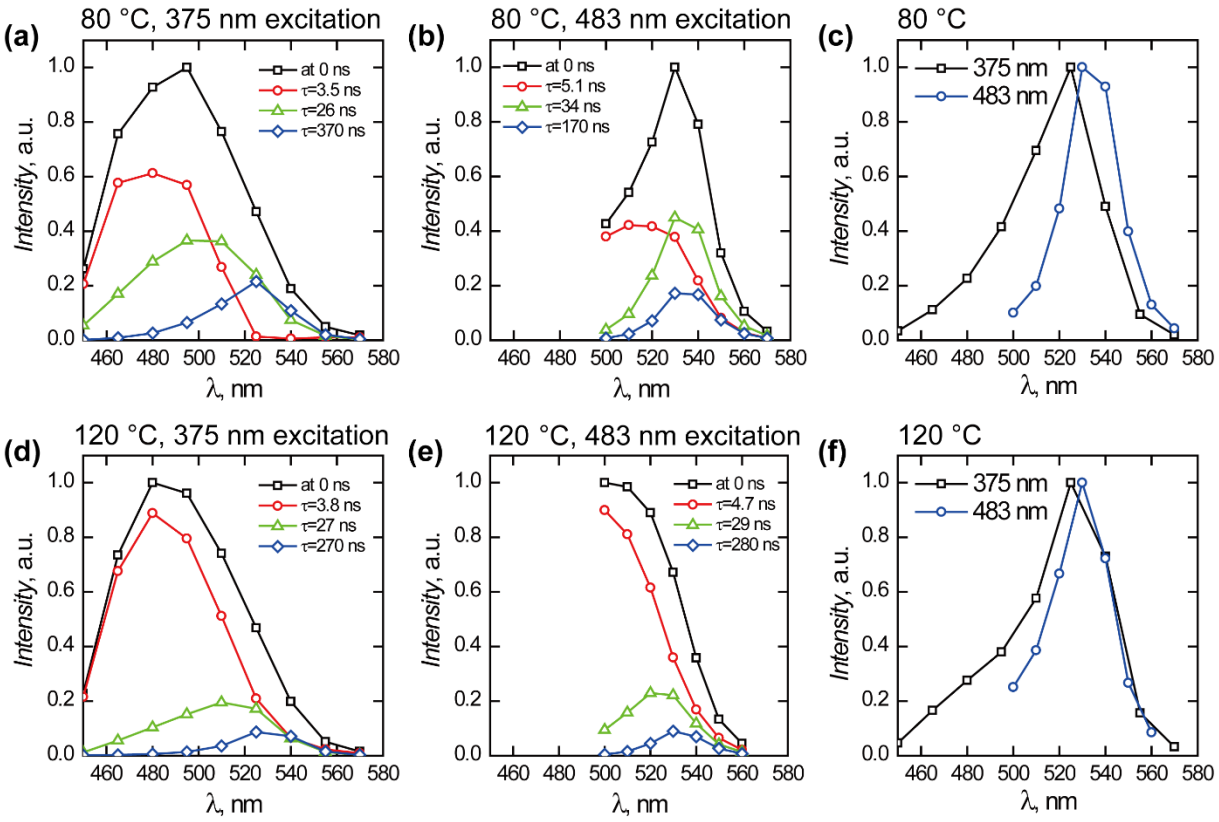

Figure S14. Decay Associated Spectra (DAS) of R = 2, 80 °C and R = 2, 120 °C-annealed case with different excitation wavelengths (375 and 483 nm). The black curve labelled at 0 ns, which is the summation of three decay curves, shows what the emission spectrum would look like immediately after the excitation. Note that the spectrum of the fastest decay component becomes more red-shifted in the 80 °C-annealed case at 483 nm excitation, compared to the 120 °C case. (c) and (f) are the recreated steady state spectra following formulae: $S = \sum a_i * \tau_i$ since steady state photoluminescence is the time integral of the emission decays at different wavelengths. The recreated steady state spectra are quite well matched with the measured steady state PL spectra.

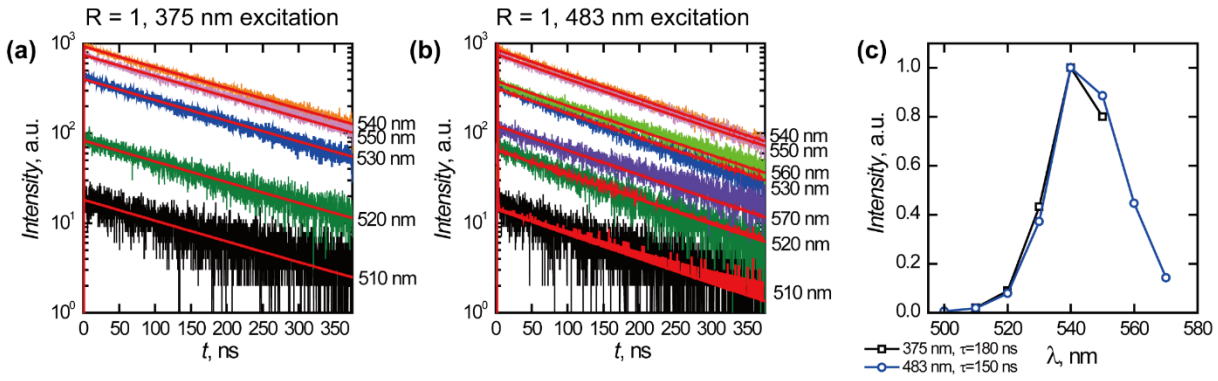

Figure S15. TRPL (Time-resolved photoluminescence lifetime) with different monitoring wavelengths with different excitation wavelengths (375 nm for a, and 483 nm for b) in R = 1 sample. (c) Recreation of steady-state PL spectrum by summation of intensities of decay components in TRPL.

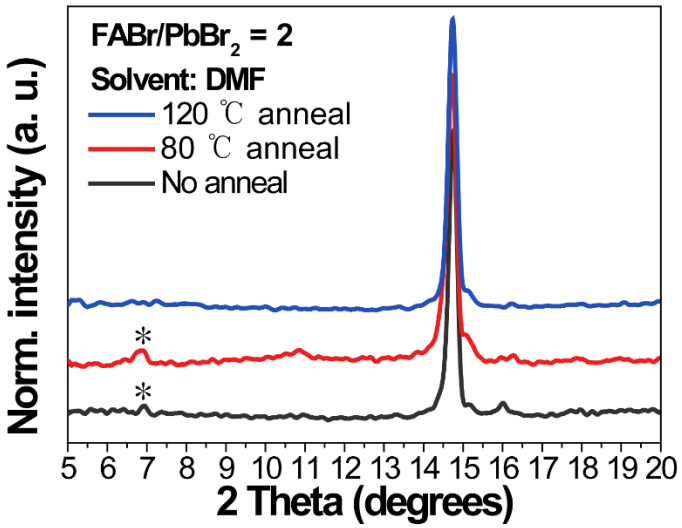

Figure S16. X-ray diffraction (XRD) patterns of the perovskite films (R = 2) using DMF as the solvent under different annealing conditions (no anneal, 80 °C and 120 °C). The marked (*) peaks represent the FA_2PbBr_4-DMSO phase

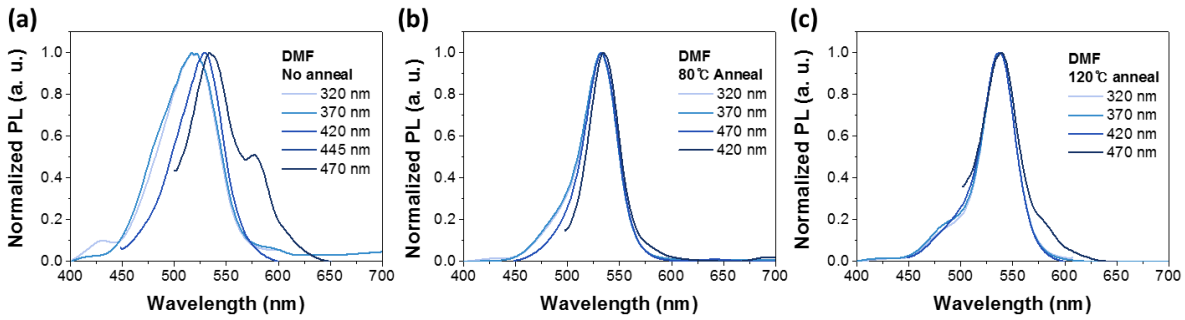

Figure S17. Normalized steady-state PL spectra from films (R = 2) using DMF as the solvent at different excitation wavelengths (λ_{exc} = 320, 370, 420 and 470 nm). (a) No annealing (dried at room temperature), (b) annealed at 80 °C and (c) annealed at 120 °C

REFERENCES

1. W. Kohn and L. J. Sham, *Phys. Rev.*, 1965, **140**, A1133– A1138.

2. G. Kresse and J. Furthmüller, *Phys. Rev. B: Condens. Matter Mater. Phys.*, 1996, **54**, 11169–11186.

3. G, Kresse and J. Furthmüller, *Comput. Mater. Sci.*, 1996, **6**, 15–50.

4. G. Kresse and D. Joubert, *Phys. Rev. B: Condens. Matter Mater. Phys.*, 1999, **59**, 1758–1775.

5. P. E. Blöchl, *Phys. Rev. B: Condens. Matter Mater. Phys.,* 1994, **50**, 17953–17979.

6. J. P. Perdew, A. Ruzsinszky, G. I. Csonka, O. A. Vydrov, G. E. Scuseria, L. A. Constantin, X. Zhou and K. Burke, *Phys. Rev. Lett.*, 2008, **100**, 136406.

7. J. Heyd, G. E. Scuseria and M. Ernzerhof, *J. Chem. Phys.*, 2003, **118**, 8207–8215.

8. A. V. Krukau, O. A. Vydrov, A. F. Izmaylov and G. E. Scuseria, *J. Chem. Phys.*, 2006, **125**, 224106.

9. K. T. Butler, J. M. Frost and A. Walsh, *Mater. Horiz.*, 2015, **2**, 228–231.

10. A. Samanta, *J. Phys. Chem. B,* 2006, **110**, 13704-13716.

11. S. K. Cushing, M. Li, F. Huang and N. Wu, *ACS nano,* 2013, **8**, 1002-1013.

12. S. Haldar, A. Chaudhuri and A. Chattopadhyay, *J. Phys. Chem. B,* 2011, **115**, 5693-706.